CrossMark

Photo-degradation of acid blue, black and brown: photo catalyst and magnetic investigation of $CoFe_2O_4$–SnO_2 nanoparticles and nano composites

Fatemeh Sadeghpour[1] · Gholamreza Nabiyouni[1] · Davood Ghanbari[2]

Abstract At the first step $CoFe_2O_4$ nanoparticles were prepared via precipitation method and at the second step $CoFe_2O_4$–SnO_2 nanocomposites were synthesized by a fast sono-chemical method. The prepared products were characterized by X-ray diffraction, scanning electron microscopy, and Fourier transform infrared spectroscopy. Magnetic property studies of the products were carried out using an alternating gradient force magnetometer and the results illustrated either ferromagnetic or super-paramagnetic behaviour of $CoFe_2O_4$ nanoparticles. The photocatalytic behaviour of $CoFe_2O_4$–SnO_2 nanocomposites was evaluated using the degradation of four various azo dyes under ultraviolet light irradiation. The results show these nanocomposites have applicable magnetic and photocatalytic performance.

1 Introduction

Nanosized spinel ferrite particles have attracted considerable interest, and many efforts continue to investigate them for their technological applications in the microwave industries, magnetic recording, refrigeration systems, ferro-fluids, MRI imaging, high frequency devices, biomedicine, catalysis, magnetic refrigerators, preparation of the information storage system, high-density ferrites at low temperatures and suspension materials in ferromagnetic liquid [1–3]. During the past decades, spinel ferrite nanoparticles have aroused growing interest in fundamental research area as well as in their potential applications in industrial, technological and biomedical field [4]. Spinel structure generally allows the introduction of different metallic ions, which can change the magnetic and electrical properties considerably. Spinel ferrites, with the general formula of MFe_2O_4, where M is a divalent cation, offer more interesting catalytic activities compared to the corresponding single component metal oxides [5]. Spinel ferrite nanocrystals are regarded as one of the most important inorganic nanomaterials because of their electronic, optical, thermal strengths, and chemical properties, as well as having cubic magnetocrystalline anisotropy [6], moderate saturation magnetization, and electrical insulation, all of which are different from their bulk counterparts. Ferrites with general structure of: $[A^{2+}]$ tetra $[B^{3+}]$ octa O_4, are well known for their electrical, magnetic and catalytic properties [3]. In a spinel structured the unit cell contains 32 oxygen atoms in cubic close packing with 8 tetrahedral (A) and 16 octahedral (B) occupied sites [1–5].

Cobalt ferrite ($CoFe_2O_4$), a cubic spinel ferrite, is largely studied in the search for improved properties and new applications; has gained its prominence due to its high coercivity (Hc), moderate saturation magnetization (Ms) [7, 8], good chemical stability and high mechanical hardness [8]. Bulk cobalt ferrite possesses inverse spinel structure. It has half of the Fe^{3+} ions on the A site (tetrahedral) and remaining half of the Fe^{3+} ions and all the Co^{2+} metal ions situate on the B-site (octahedral). Synthesis of this material in nano-regime induces cation redistribution over A and B sites in the spinel ferrite which leads to magnetic properties different from its bulk counterpart [9].

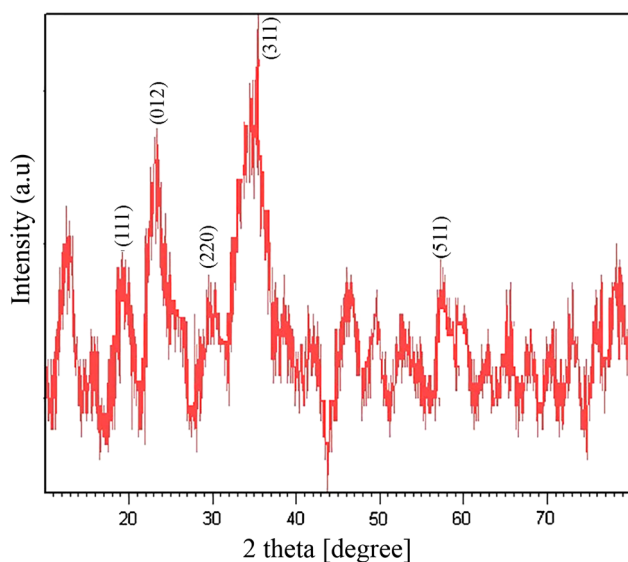✉ Gholamreza Nabiyouni
G-nabiyouni@araku.ac.ir

1 Department of Physics, Faculty of Science, Arak University, Arak 38156-88349, Iran

2 Young Researchers and Elite Club, Arak Branch, Islamic Azad University, Arak, Iran
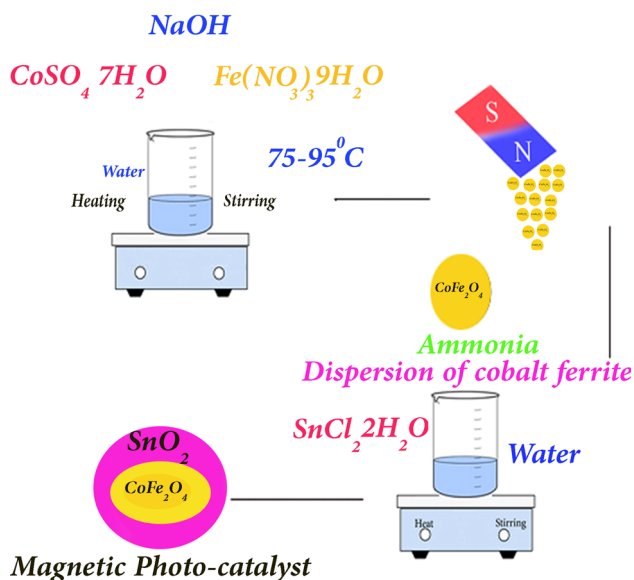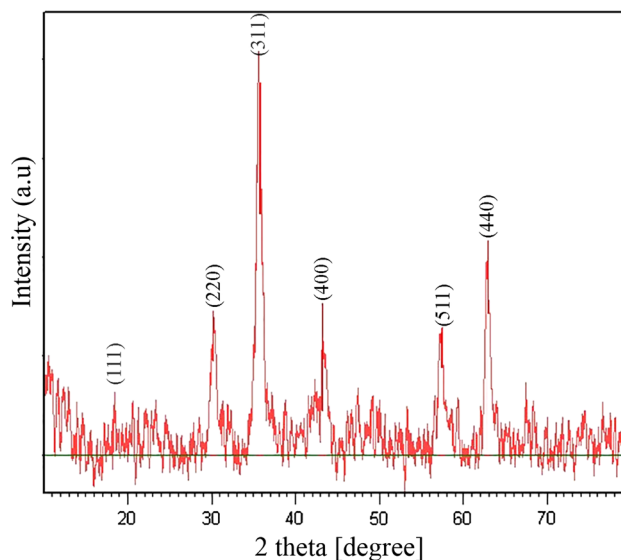
Fig. 1 Schematic of nanocomposite preparation

Fig. 3 XRD pattern of CoFe$_2$O$_4$ nanoparticles (95 °C)

Thus nanosized CoFe$_2$O$_4$ is neither completely normal nor completely inverse spinel, but has mixed spinel structure [9]. In the pure cobalt ferrite, half of the Fe^{3+} ions reside in the tetrahedral sites while remaining ions seek to the octahedral sites [10]. Owing to the above properties, it is a promising candidate for high density recording media, bio-medical drug delivery, cancer treatment, magnetic resonance imaging, catalysis, telecommunications, UV and visible light induced photocatalysts, anode materials, support for magnetic fluids, microwave devices, etc. [8–13]. Magnetic characteristic of cobalt ferrites allows them to be employed as heterogeneous catalysts, which can be easily

recovered from the reaction mixture using an external magnet. Therefore, it has been exploited as catalyst in a variety of organic transformations [12, 13]. These properties depend on their chemical composition and nanostructures characteristics, where the particle size and shape might be controlled in the fabrication processes [6, 13]. Various preparation techniques have been developed so far to synthesize spinel ferrite nanostructures such as sol–gel, mechno-synthesis, solvothermal, co-precipitation techniques, and micro-emulsions. However, to obtain a controllable synthesis of mono-dispersed ferrite particles and to establish the correlation between synthetic conditions and magnetic properties are still the most important challenges and research topics of spinel ferrite nanomaterials [10–15]. It is well known that the chemical, structural, and


Fig. 2 XRD pattern of CoFe$_2$O$_4$ nanoparticles (75 °C)
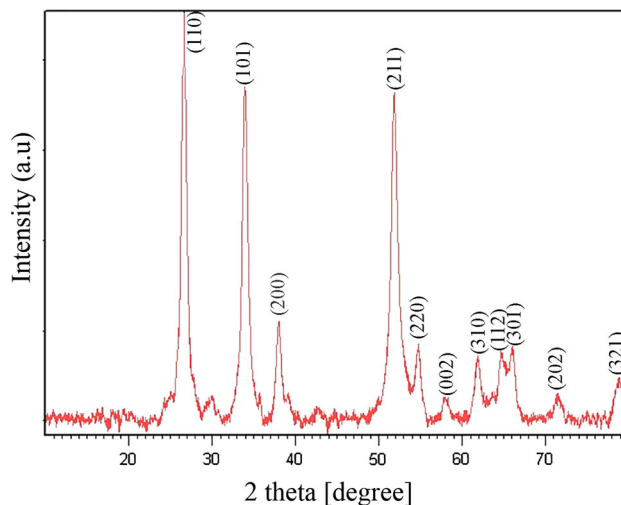
Fig. 4 XRD pattern of SnO$_2$ nanoparticles
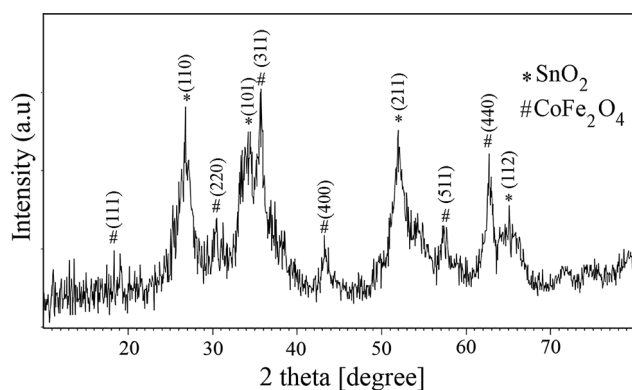
Fig. 5 XRD pattern of CoFe$_2$O$_4$–SnO$_2$ (50 %:50 %) nanocomposite

magnetic properties of ferrite nanoparticles are greatly influenced by their composition and nanostructures, which are sensitive to their synthesis method [4, 15]. Among the processes, the co-precipitation method has been further developed because of its simplicity, suitable, low cost, nontoxic precursors, non-time-consuming, and industrial scale yielding. However, in this method, the insignificant control of size during synthesizes process still is a main challenge. It is known that the particle size and crystallinity can be controlled by adjusting the supersaturation during the nucleation and crystal growth processes, which in turn, it can strongly be affected by solution chemistry and precipitation conditions such as reaction temperature and pH of process environment [16, 17].

Semi conductor nanoparticles have been studied from both experimental and theoretical viewpoints, owing to their potential applications in solar energy conversion, photocatalysis and optoelectronic industry. SnO$_2$ is an important n-type semiconductor, which presents a proper combination of electronic and optical properties. It has several applications such as transparent conducting films, catalytic materials, environmental monitoring, sensor, dye-sensitized solar cells and optical electronic devices. Various methods such as microwave heating, ball milling, sono-chemical, solvo-thermal, precipitation, sol–gel, chemical vapour deposition and thermal evaporation have been investigated. Considerable investigations have been focused on the synthesis of SnO$_2$ nanostructures with various morphologies including hollow-spheres, core–shell, flower-like, nanowires, nano-tubes, nano-belts and meso-porous [18–23]. In this work CoFe$_2$O$_4$–SnO$_2$ nanocomposites were synthesized by precipitation method. The photo catalytic behaviour of CoFe$_2$O$_4$–SnO$_2$ nanocomposites was evaluated using the degradation of four various azo dyes under ultraviolet light irradiation. The results show that nanocomposites have applicable super paramagnetic and photo catalytic performance.
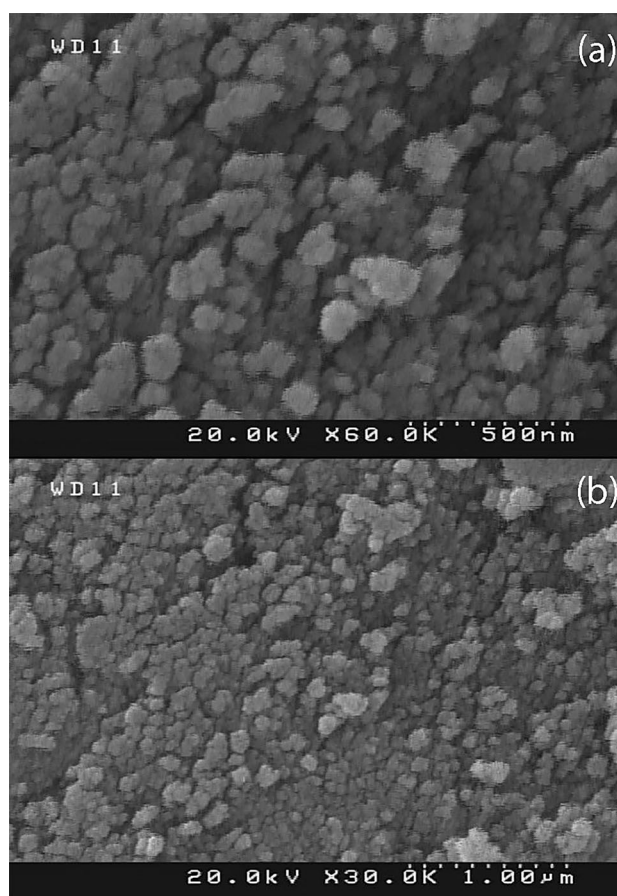

Fig. 6 SEM images of CoFe$_2$O$_4$ without surfactant

2 Experimental

2.1 Materials and methods

Fe (NO$_3$)$_3$·9H$_2$O, CoSO$_4$·7H$_2$O, NaOH, NH$_3$, lactose, sodium dodecyl sulphate (SDS), polyvinyl alcohol (PVA), cetyl trimethyl bromide) CTAB (, distilled water and SnCl$_2$·2H$_2$O were purchased from Merck company. XRD patterns were recorded by a Philips, X-ray diffractometer using Ni-filtered CuK$_\alpha$ radiation. SEM images were obtained using a LEO instrument model 1455VP. All the chemicals were used as received without further purifications. Prior to taking images, the samples were coated by a very thin layer of Pt (using a BAL-TEC SCD 005 sputter coater) to make the sample surface conductor and prevent charge accumulation, and obtaining a better contrast. Room temperature magnetic properties were investigated using an alternating gradient force and vibrating sample magnetometers (AGFM and VSM) device (Meghnatis Kavir Kashan Co., Iran) in an applied magnetic field sweeping between ±10,000 Oe. A multiwave ultrasonic generator (Bandeline MS 73), equipped with a converter/transducer and titanium oscillator, operating at 20 kHz with a
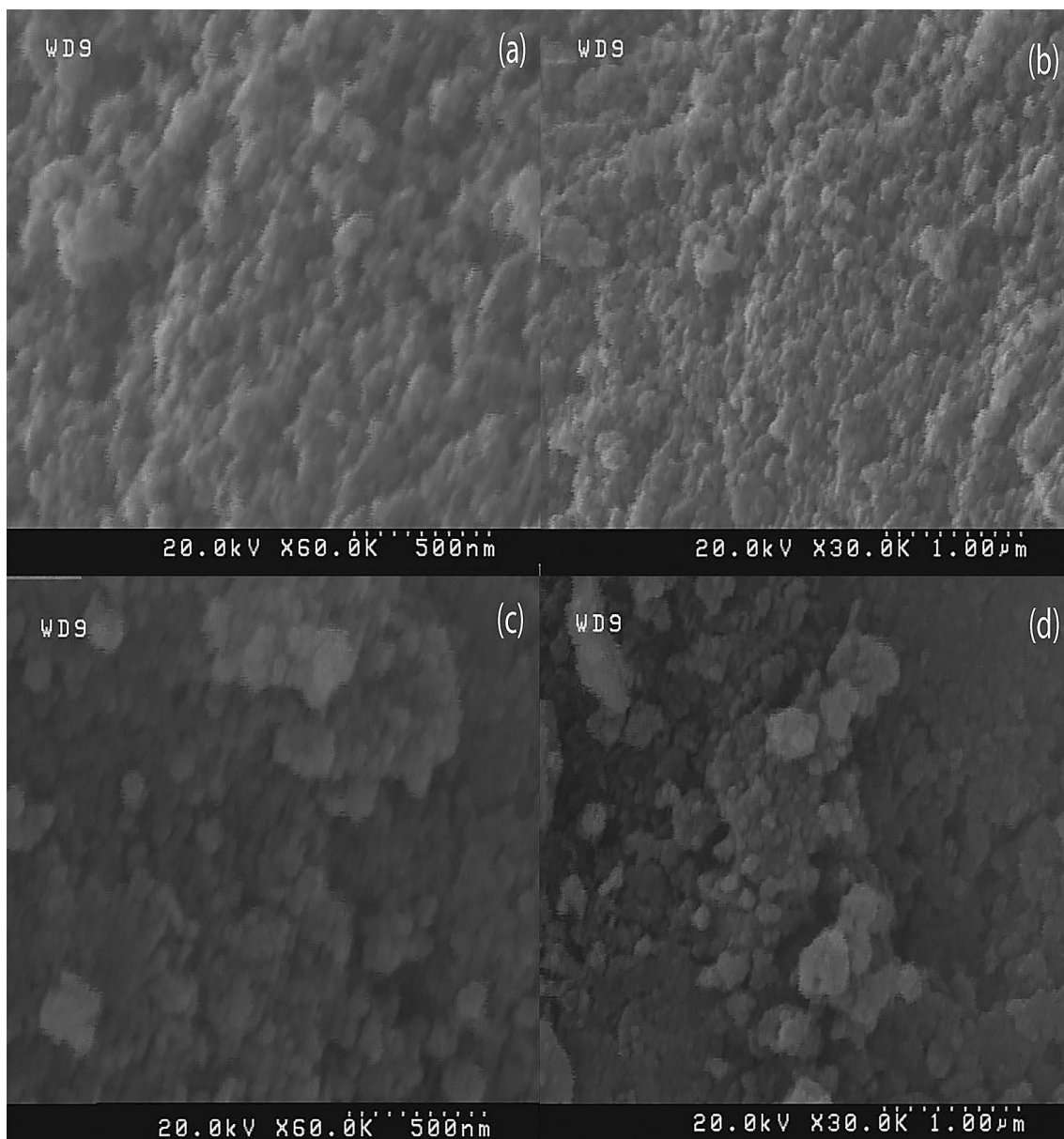
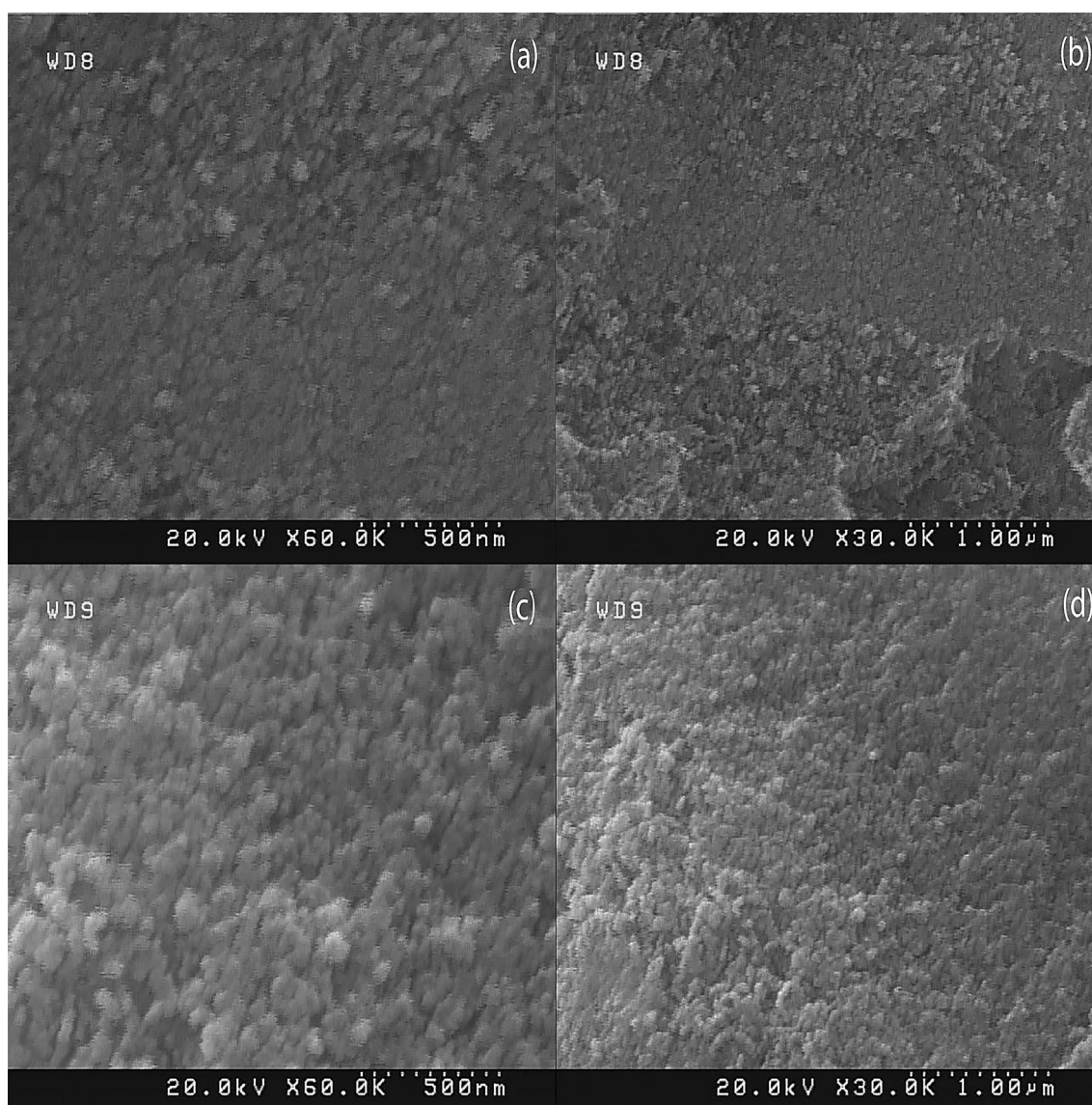**Fig. 7** SEM images of CoFe$_2$O$_4$ prepared at 75 °C by **a**, **b** CTAB, **c**, **d** SDS

maximum power output of 150 W was used for the ultrasonic irradiation.

2.2 Synthesis of CoFe$_2$O$_4$ nanoparticles

Firstly 0.58 g of Fe (NO$_3$)$_3$·9H$_2$O and 0.2 g of CoSO$_4$·7H$_2$O was dissolved in 175 ml of distilled water. Then 0.05 g of SDS as anionic surfactant was added to the solution. It was mixed on magnetic stirring for 10 min. Then 8 ml of NaOH (1 M) as precipitator was slowly added to raising solution pH to 10. The solution was then heated at temperature of 75 °C for 1 h. The obtained black precipitate was washed twice with distilled water. Then it was dried in oven for 24 h. Same procedure was done for synthesis the one more sample except that 1 ml of ammonia was used as a precipitating agent.
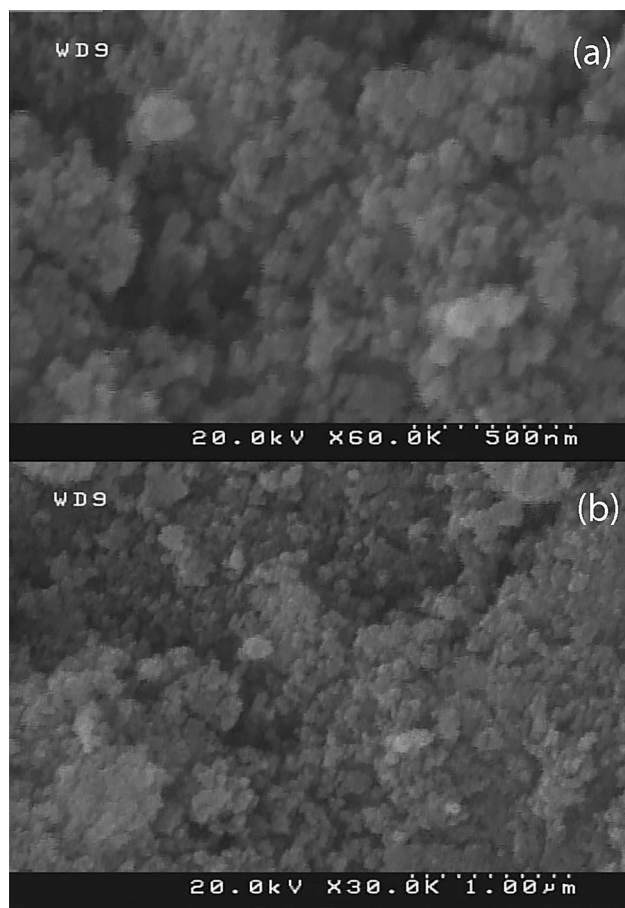
Fig. 8 SEM images of CoFe$_2$O$_4$ prepared by **a**, **b** lactose, **c**, **d** PVA

2.3 Synthesis of CoFe$_2$O$_4$–SnO$_2$ (50 %:50 %) nanocomposites

Firstly 0.2 g of synthesized cobalt ferrite was dispersed in 100 ml of distilled water. Then 0.4 g of SnCl$_2$ added to the solution (under ultra sonic waves 140 W, 30 min) and was mixed for 2 h. After that 1 ml of NH$_3$ was slowly added to reaching solution pH to 10, then the solution was stirred for 1 h. The sample was dried in oven for 24 h and calcinated at 400 °C for 2 h (Fig. 1).

2.4 Photo-catalytic degradation process

10 ml of the dye solution (20 ppm) was used as a model pollutant to determine the photocatalytic activity. 0.1 g of catalyst was applied for degradation of 10 ml solution. The solution was mixed by a magnet stirrer for 1 h in darkness to determine the adsorption of the dye by catalyst and better availability of the surface. The solution which was stirred and placed in a quartz pipe was located in the middle of reactor and was irradiated for 2 h by a

Fig. 9 SEM images of $CoFe_2O_4$ prepared by ammonia (without surfactant)

10 W UV lamp. The samples were finally filtered, centrifuged. Their concentration was determined by UV–visible spectrometry.

3 Results and discussion

Figure 2 illustrates XRD pattern of $CoFe_2O_4$ product obtained at 75 °C. The effect of temperature on the crystallinity was investigated and the pattern confirms that the better crystallization was obtained at higher synthesize temperature. This result agrees with magnetic outcomes which says increasing the synthesize temperature (up to 600 °C), leads to preparation of magnetic samples with higher magnetization and coercivity. It seems pure crystallite lattice of cobalt ferrite was synthesized at temperature higher than 90 °C. Figure 3 illustrates XRD pattern of $CoFe_2O_4$ product obtained at 95 °C. It can be observed that structural phase of face centered cubic (JCPDS No. 22-1086, space group: Fd3 m) is present in the pattern.

Figure 4 shows XRD pattern of SnO_2 product. Tetragonal phase (with JCPDS: 41-1445, space group: P42/mnm) is presented in the pattern.

The composition of the $CoFe_2O_4$–SnO_2 nanocomposite was investigated by XRD pattern and it is depicted in Fig. 5. All calcined samples exhibit diffraction peaks consistent with both spinel cubic structure of (22-1086) and tetragonal tin dioxide (JCPDS: 41-1445) with no evidence of any impurity phases. The peak intensities related to each counterpart is relatively similar which indicates of rather equal portion of the shared compounds in the composite. The crystalline sizes was calculated from Scherrer equation, $D_c = K\lambda/\beta Cos\theta$, where β is the width of the observed diffraction peak at its half maximum intensity (FWHM), K is the shape factor, which takes a value of about 0.9, and λ is the X-ray wavelength (CuK_α radiation, equals to 0.154 nm). The values of about 2 and 10 nm were found for crystalline sizes of $CoFe_2O_4$ and $CoFe_2O_4$–SnO_2 nanoparticles, respectively. Figure 6 illustrates SEM images (in two magnifications) of the as-synthesized and surfactant-free $CoFe_2O_4$ nanoparticles (synthesized at 75 °C). The image demonstrates nanoparticles with average diameter of less than 70 nm. This reaction was chosen as basic reaction and effect of changing various parameters on this reaction was investigated.

SEM images of $CoFe_2O_4$ by Cetyltrimethyl bromide (CTAB) as a cationic surfactant at 75 °C are shown in Fig. 7a, b. The Images confirm synthesize of products with particle size around 50 nm. SEM images of $CoFe_2O_4$ synthesized by sodium dodecyl sulphate (SDS) as anionic surfactant at temperature of 75 °C are illustrated in Fig. 7c, d. The average particle size is about 60 nm.

Effect of lactose as a green, safe and cost-effective capping agent was also examined. SEM images of $CoFe_2O_4$ prepared by lactose at 400 °C are shown in Fig. 8a, b. The images approve product with mediocre size around 45 nm. Figure 8c, d show images of magnetic ferrite obtained by poly vinyl alcohol as neutral capping agent and illustrate preparation of nanoparticles (their size is around 40 nm).

Precipitating agent was then changed from sodium hydroxide to ammonia. SEM images of $CoFe_2O_4$ prepared with ammonia at temperature 650 °C are shown in Fig. 9 and confirms that mono disperse nanoparticles (with average size of about 50 nm) were synthesized.

Figure 10a, b illustrate SEM images of $CoFe_2O_4$ prepared at 75 °C, by cethyl trimethyl ammonium bromide as conventional surfactant, and the smallest nano particles were achieved. The magnetic product obtained by sodium do decyl solfate at 75 °C (Fig. 10c, d). The mono-disperse and uniform nanoparticles (less than 35 nm) were achieved.
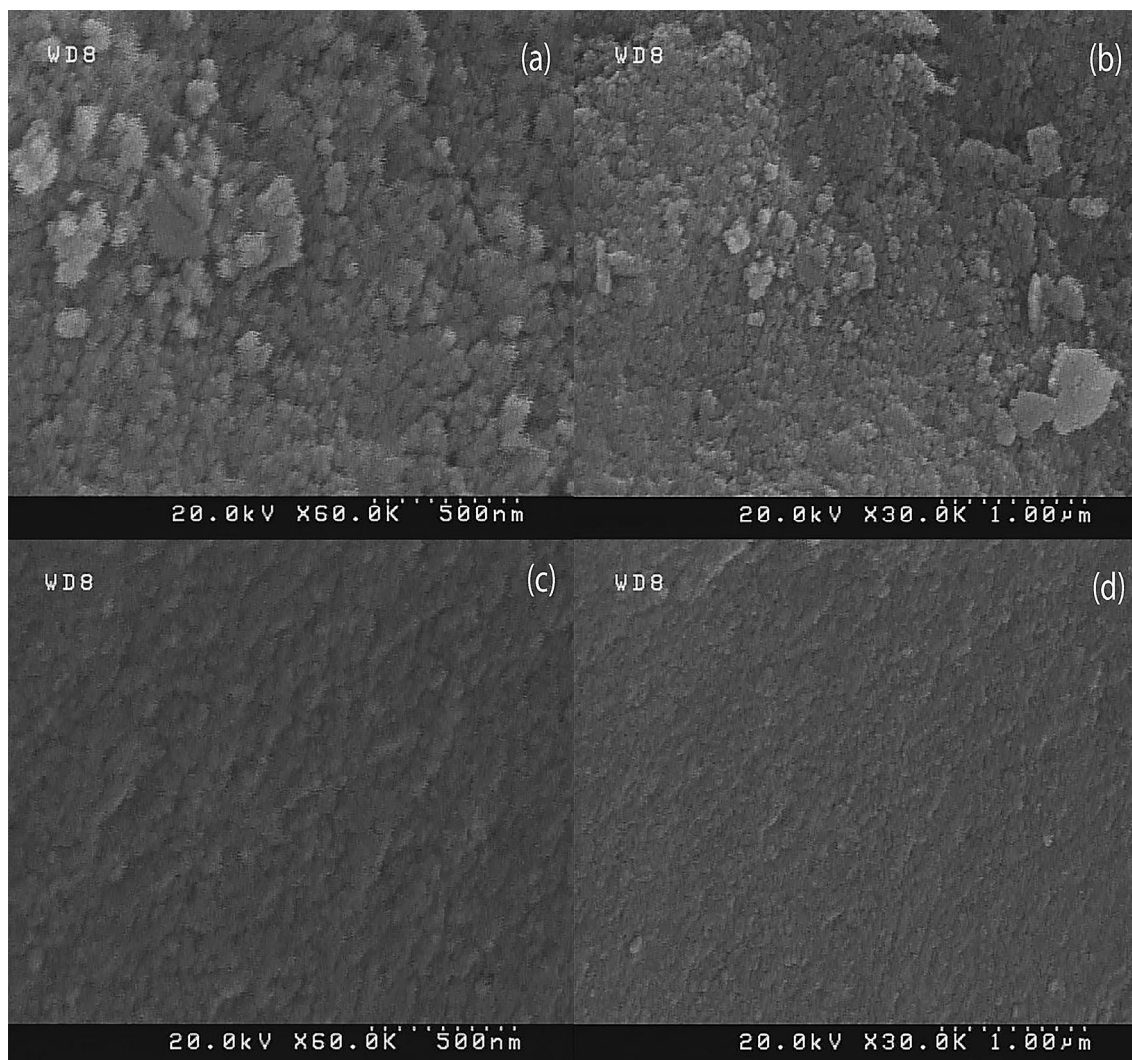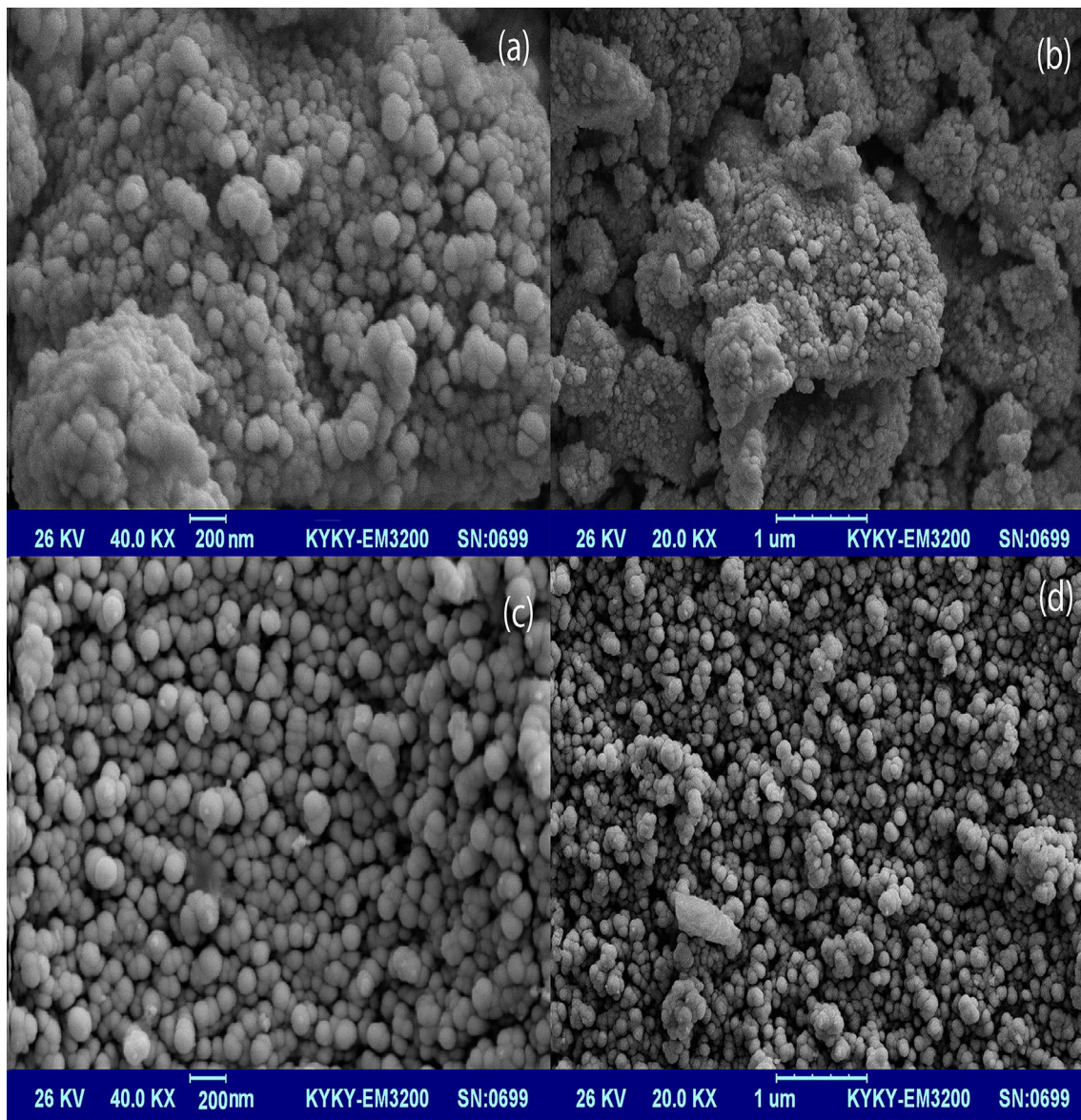
Fig. 10 SEM images of $CoFe_2O_4$ prepared by ammonia at 75 °C: **a**, **b** CTAB, **c**, **d** SDS

Influence of precursors was examined and iron nitrate was replaced to iron chloride, Fig. 11a, b depict SEM images of $CoFe_2O_4$ prepared by $FeCl_3 \cdot 6H_2O$ at 75 °C, it shows 40 nm magnetic product were obtained. Cobalt source was replaced from sulphate to acetate. Figure 11c, d depict SEM images of $CoFe_2O_4$ prepared by cobalt acetate. It seems the best mono-disperse nanoparticles were synthesized by acetate salt. SEM images of as-synthesized SnO_2 are shown in Fig. 12, and outcomes confirm nanoparticles with average size of around 40–50 nm were achieved.

SEM images of $CoFe_2O_4$–SnO_2 nanocomposite are illustrated in Fig. 13 nanostructures with grain size about 50 nm were synthesized. In both reactions the nucleation was preferential compare to crystal growth. Figure 14a–c show the FT-IR spectra of the ferrite prepared at three different temperatures of 75, 95 and 400 °C respectively.

In Fig. 14, the absorption bands around 445–550 cm^{-1} are assigned to the Co–O and Fe–O (metal–oxygen) stretching mode. The spectra exhibit broad absorption peaks around 3350–3400 cm^{-1}, corresponding to the stretching mode of O–H group of adsorbed hydroxyl group and the weak band near 1630 cm^{-1} is assigned to H–O–H bending vibration mode due to the adsorption of moisture on the surface of nanoparticles. Figure 15 illustrates the FT-IR spectrum of the as-prepared tin dioxide. The absorption bands at 550 and 625 cm^{-1} are assigned to the Sn–O stretching mode. The spectrum exhibits broad absorption peaks at 3460 cm^{-1}, corresponding to the stretching mode of O–H group. Figure 16 shows the FT-IR spectrum of the as-prepared $CoFe_2O_4$–SnO_2 nanocomposite. It can be observed that the strong absorption band around 580 cm^{-1} which are ascribed to phonon absorptions of the $CoFe_2O_4$–SnO_2 lattice and broad absorption peaks at 3427 cm^{-1} are

Fig. 11 SEM images of $CoFe_2O_4$ prepared by NaOH **a**, **b** $FeCl_3 \cdot 6H_2O$, **c**, **d** cobalt acetate

assigned to adsorbed O–H groups on the surface of nanoparticles. There are no other significant peaks related to precursors and other impurities.

Room temperature magnetic properties of samples were studied using alternating gradient force magnetometer (AGFM) system. Hysteresis loop of magnetic $CoFe_2O_4$ nanoparticles at 75 °C is shown in Fig. 17. As-synthesized nanoparticles show super paramagnetic behaviour and have a saturation magnetization of 4.3 emu/g and a coercivity about zero Oe.

Hysteresis curve of magnetic $CoFe_2O_4$ nanoparticles at 400 °C (at present of lactose) is shown in Fig. 18. As-synthesized nanoparticles exhibit nearly paramagnetic behaviour with a small coercivity of about 12 Oe.

Hysteresis loop of magnetic $CoFe_2O_4$ nanoparticles at 650 °C is shown in Fig. 19. As-synthesized nanoparticles exhibit ferromagnetic behaviour (in fact they are ferrimagnets) and show a saturation magnetization of 27 emu/g and a coercivity about 390 Oe. Hysteresis loop of magnetic $CoFe_2O_4$ nanoparticles by ammonia is shown in Fig. 20. As-prepared nanoparticles show ferromagnetic behaviour and have a saturation magnetization of 60 emu/g and a coercivity tends to 1076 Oe. Hysteresis loop of magnetic $CoFe_2O_4$–SnO_2 nanocomposite is shown in Fig. 21. As-prepared nanocomposite show ferromagnetic behaviour and have a saturation magnetization of 2 emu/g and coercivity tends to 35 Oe. This magnetization indicates that $CoFe_2O_4$–SnO_2 nanocomposites inherit
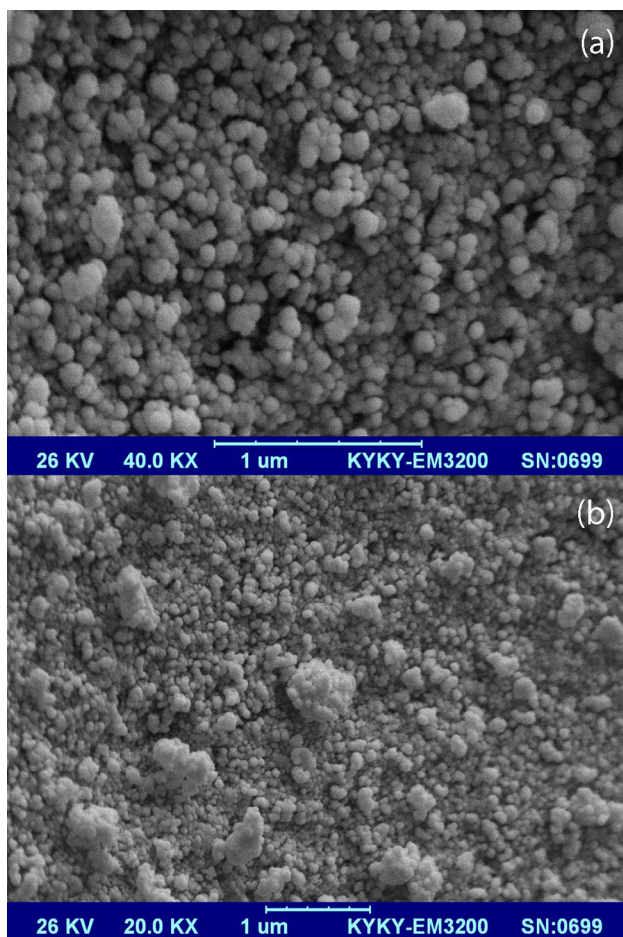
**Fig. 12** SEM images of SnO_2 nanoparticles
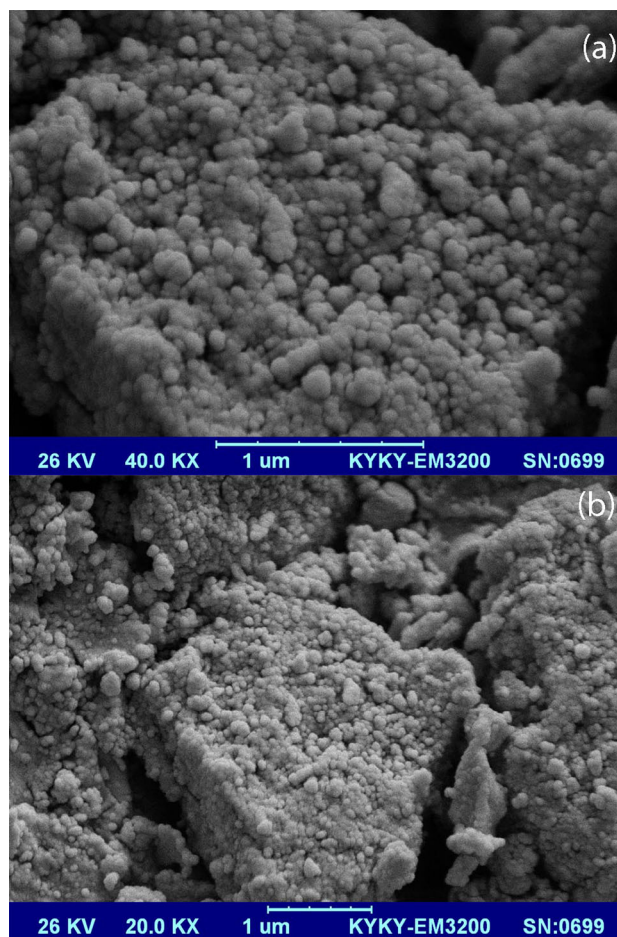
Fig. 13 SEM images of $CoFe_2O_4$–SnO_2 nanocomposite

the magnetic property from the $CoFe_2O_4$. However, their magnetization is lower because of presence of tin dioxide. This reduction in saturation magnetization is due to the interfacial effect of the typical nanocomposite. It shows a sufficient magnetization of these nanoparticles for being recycled by a magnet, making them appropriate for core of recyclable photocatalyst. The photo-catalytic activity of the $CoFe_2O_4$–SnO_2 nanocomposite was evaluated by monitoring the degradation of Acid black, Acid brown, Acid blue and Congo red as aqueous solutions under irradiation with UV light. The mechanism of

photocatalytic activity of nano-composite is shown in Fig. 22. The changes in the concentration of dye are illustrated in Figs. 23 and 24. Acid black, Acid blue, Acid brown and Congo red were degraded about 90, 95, 85 and 99 % respectively in 120 min. Organic dyes decompose to carbon dioxide, water and other less toxic or nontoxic residuals [24–26]. Differences between our previous work ($CuFe_2O_4$–TiO_2) and $CoFe_2O_4$–SnO_2 are shown in Table 1 [24]. Figure 25 shows degradation of four azo dyes after 120 min exposure of UV at presence of $CoFe_2O_4$–SnO_2 nanocomposite.
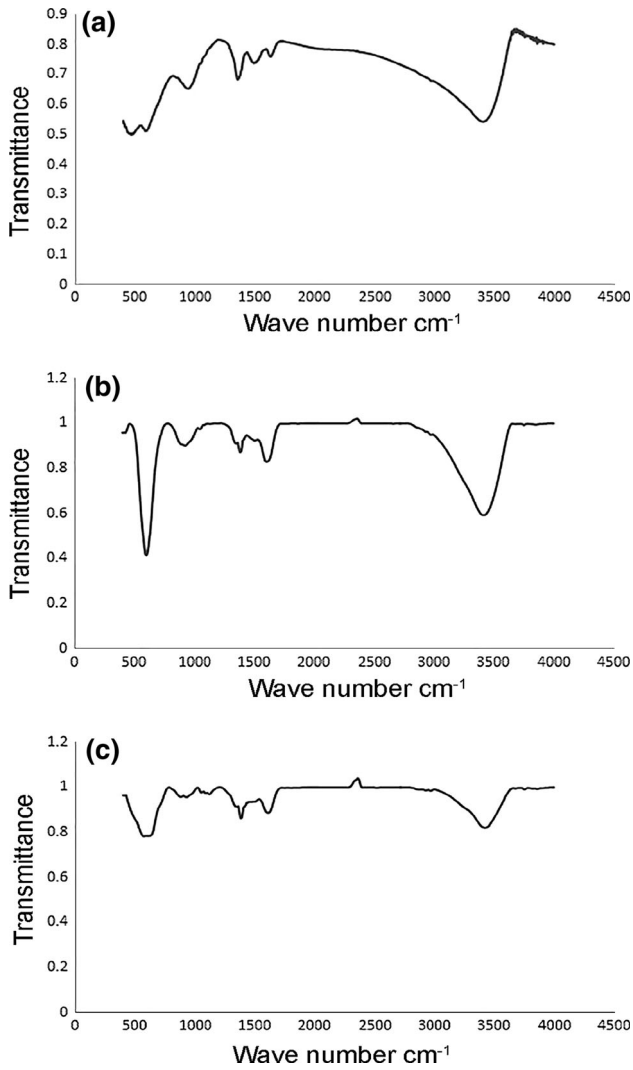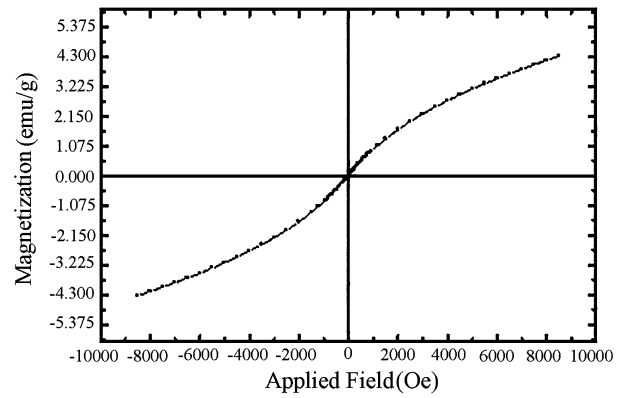
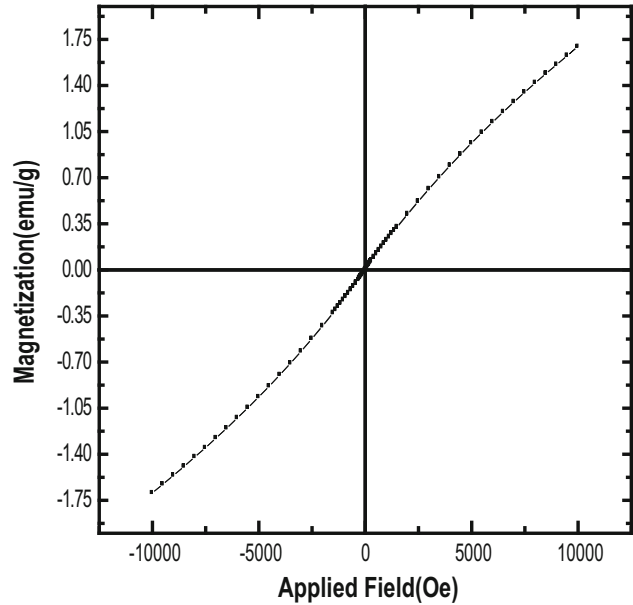Fig. 14 FT-IR spectra of CoFe$_2$O$_4$ nanoparticles at **a** 75 °C, **b** 95 °C, **c** 400 °C
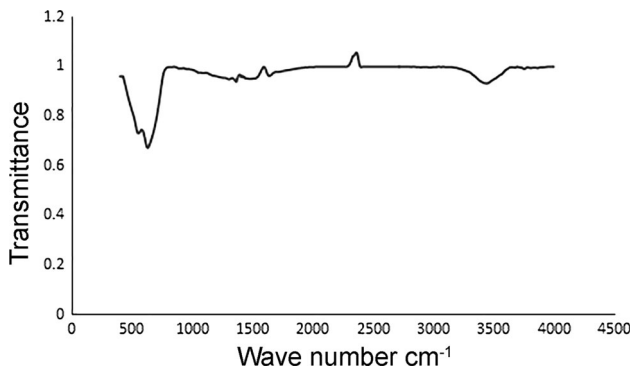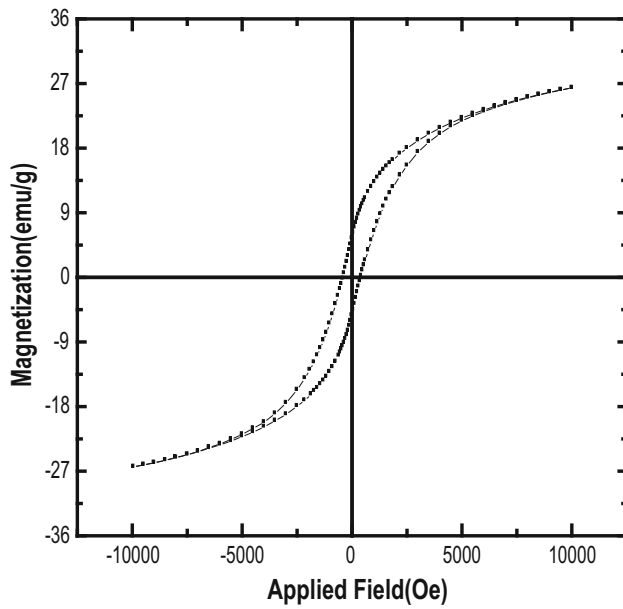

Fig. 15 FT-IR spectrum of SnO$_2$ nanoparticles
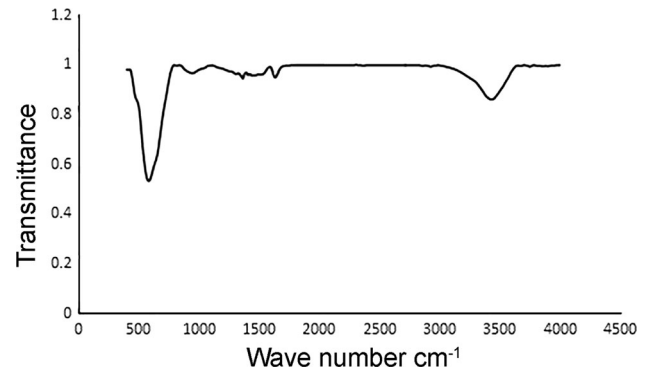
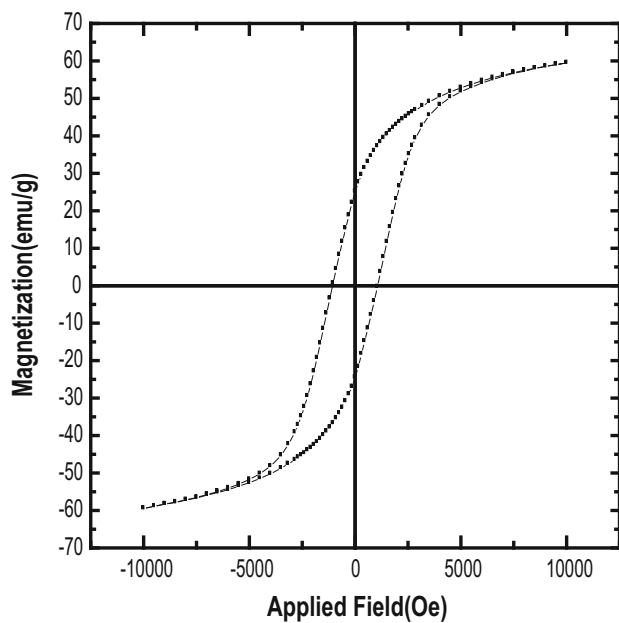Fig. 16 FT-IR spectrum of CoFe$_2$O$_4$–SnO$_2$ nanocomposite

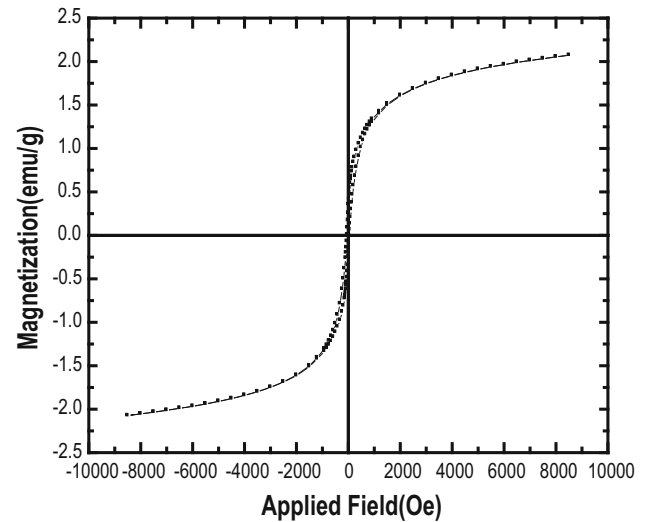Fig. 17 Room temperature hysteresis curve of CoFe$_2$O$_4$ nanoparticles (75 °C)

Fig. 18 Hysteresis curve of CoFe$_2$O$_4$ nanoparticles at 400 °C

Fig. 19 Hysteresis loop of CoFe$_2$O$_4$ nanoparticles at 650 °C

**Fig. 20** Hysteresis loop of CoFe$_2$O$_4$ nanoparticles at 650 °C (ammonia)

**Fig. 21** Hysteresis loop of CoFe$_2$O$_4$–SnO$_2$ nanocomposite

4 Conclusions

Firstly cobalt ferrite nanoparticles were synthesized via precipitation method. Then CoFe$_2$O$_4$–SnO$_2$ nanocomposites were prepared via a simple ultrasonic-assisted method. Effect of precipitating agent, capping agents and temperature were investigated on the morphology and particle size of the products. AGFM confirmed that various nanostructures exhibit different super-paramagnetic, para-magnetic and ferromagnetic behaviour. The photocatalytic behaviour of CoFe$_2$O$_4$–SnO$_2$ nanocomposite was evaluated using the degradation of Acid blue, Acid black, Congo red and Acid brown under UV light irradiation. The results show that precipitation and ultrasonic method are suitable method for preparation of CoFe$_2$O$_4$–SnO$_2$ nanocomposites as a candidate for photocatalytic applications.

Fig. 22 Photo-catalyst mechanism of CoFe$_2$O$_4$–SnO$_2$ nanocomposite
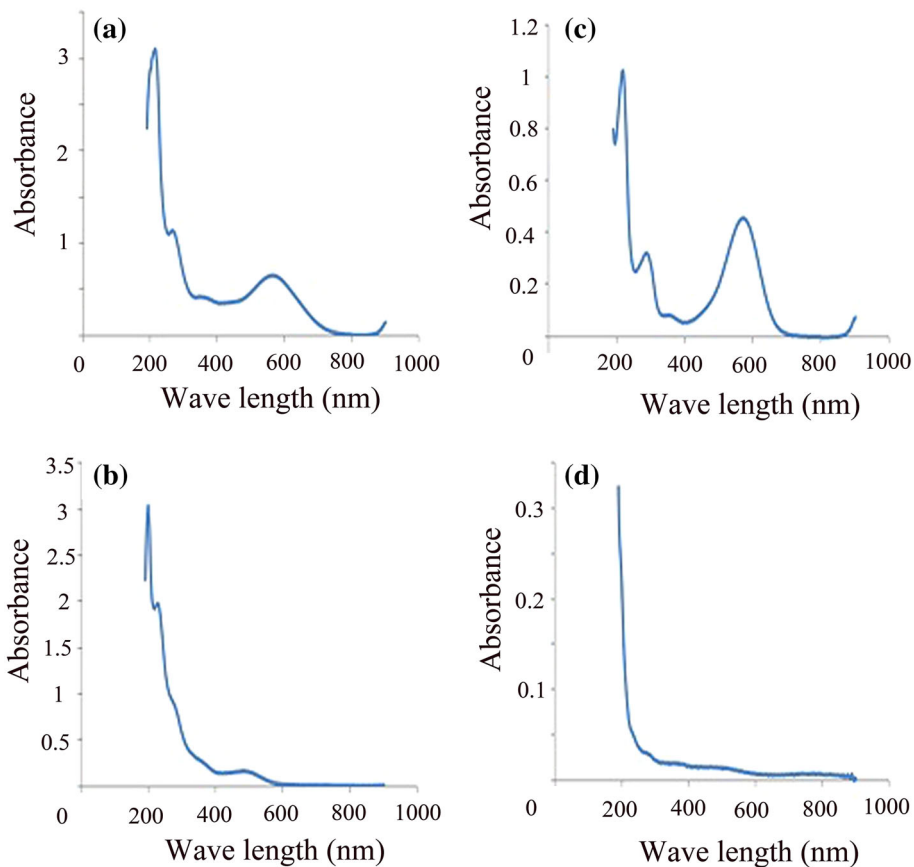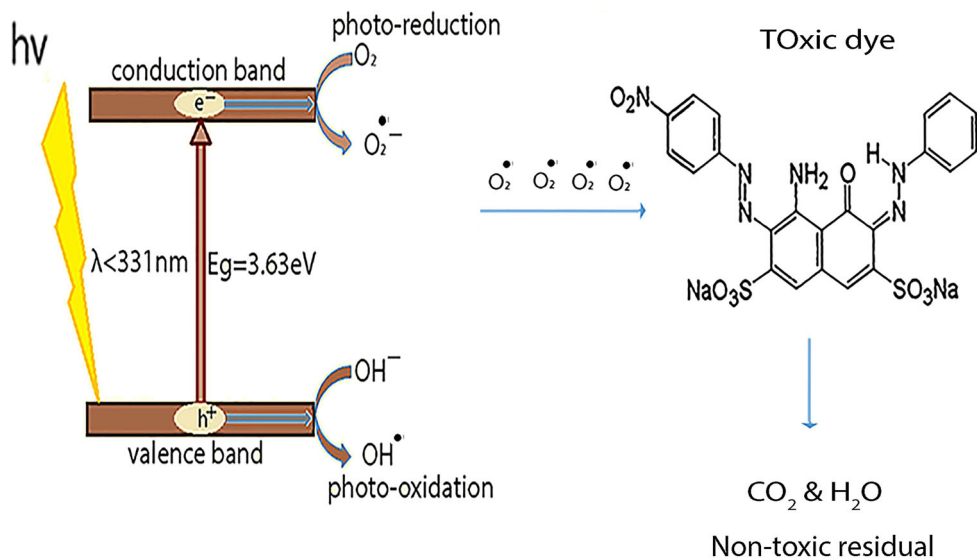
Fig. 23 UV–Vis spectrum of degradation of Acid black 1 **a** 0 min, **b** 120 min and Acid blue **c** 0 min, **d** 120 min
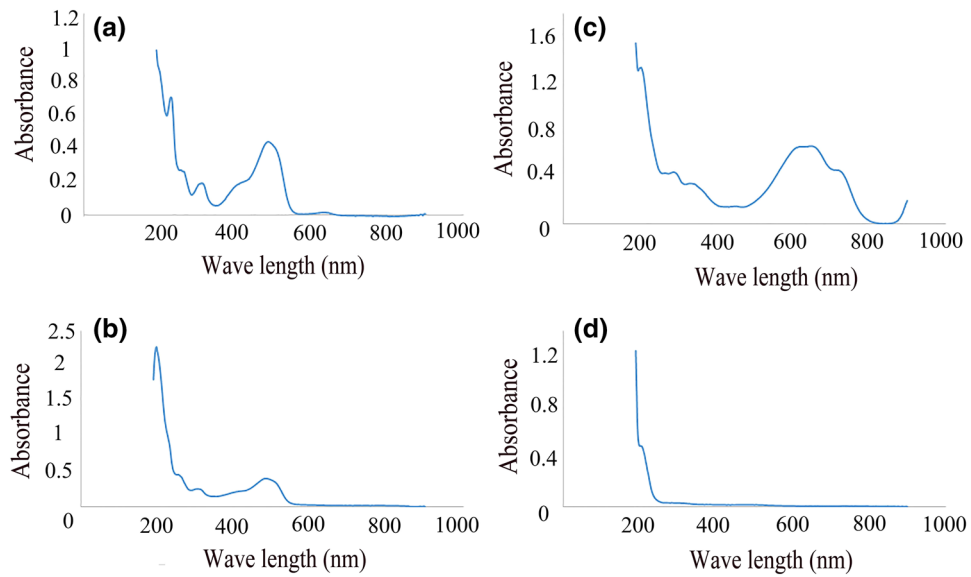
Fig. 24 Degradation of Acid brown 14 **a** 0 min, **b** 120 min and Congo red (pH = 3) **c** 0 min, **d** 120 min

Table 1 Differences between $CuFe_2O_4$–TiO_2 and $CoFe_2O_4$–SnO_2 nanocomposite

Differences	Previous work [24]	Present work
Ferrite	$CuFe_2O_4$	$CoFe_2O_4$
Surfactant	PVA and SDS	PVA, SDS, CTAB, lactose
Temperature of ferrite	200–600 °C	75–650 °C
Photo-catalyst	TiO_2	SnO_2
Preparation of photo-catalyst	Sol gel	Precipitation and sono-chemical
Temperature of photo-catalyst	500 °C	400 °C

Fig. 25 Degradation of azo-dyes at presence of $CoFe_2O_4$–SnO_2 **a** Acid black, **b** Acid blue, **c** Acid brown and **d** Congo red
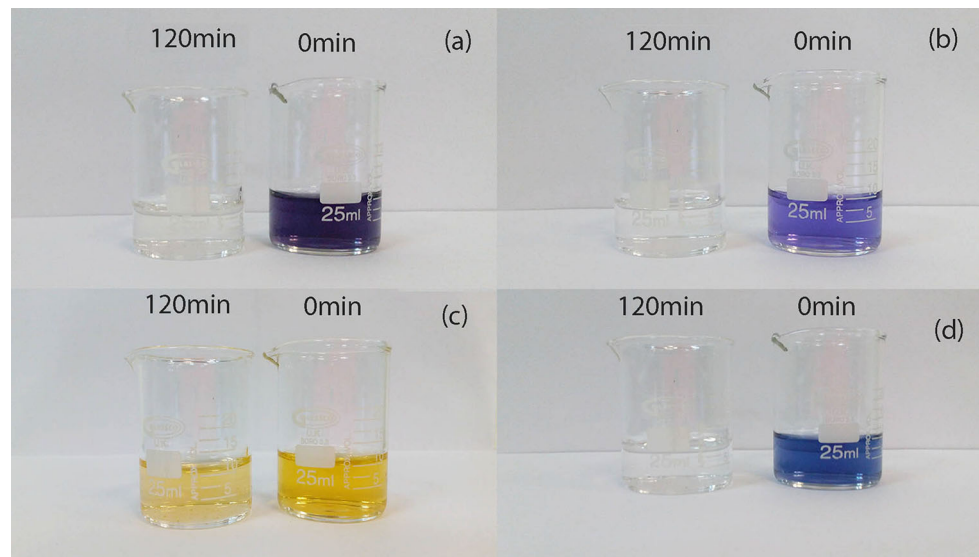
References

1. A.M. Cojocariu, M. Soroceanu, L. Hrib, V. Nica, O.F. Caltun, Mater. Chem. Phys. **135**, 728 (2012)
2. A.K. Nikumbh, R.A. Pawar, D.V. Nighot, G.S. Gugale, M.D. Sangale, M.B. Khanvilkar, A.V. Nagawade, J. Magn. Magn. Mater. **355**, 201 (2014)
3. Y. Koseoglu, F. Alan, M. Tan, R. Yilgin, M. Ozturk, Ceram. Int. **38**, 3625 (2012)
4. Z. Ding, W. Wang, Y. Zhang, F. Li, J. Ping Liu, J. Alloy. Compd. (2015). doi:10.1016/j.jallcom.2015.04.020
5. M. Kooti, M. Afshari, Sci. Iran. F **19**(6), 1991 (2012)
6. C.V. Reddy, C. Byon, B. Narendra, D. Baskar, G. Srinivas, J. Shim, S.V. Prabhakar Vattikuti, Superlattices Microstruct. **82**, 165 (2015)
7. M.B. Ali, K.E. Maalam, H.E. Moussaoui, O. Mounkachi, M. Hamedoun, R. Masrour, E.K. Hlil, A. Benyoussef, J. Magn. Magn. Mater. (2015). doi:10.1016/j.jmmm.08.097.2015
8. F. Huixia, C. Baiyi, Z. Deyi, Z. Jianqiang, T. Lin, J. Magn. Magn. Mater. **356**, 68 (2014)
9. H. Kumar, R.C. Srivastava, J.P. Singh, P. Negi, H.M. Agrawal, D. Das, K.H. Chae, J. Magn. Magn. Mater. (2015). doi:10.1016/j.jmmm.2015.09.077
10. S. Jauhar, S. Singhal, M. Dhiman, Appl. Catal. A **486**, 210 (2014)
11. L. Avazpour, M.A. Zandi Khajeh, M.R. Toroghinejad, H. Shokrollahi, J. Alloys Compd. **637**, 497 (2015)
12. A. Goyala, S. Bansalb, V. Kumarc, J. Singhd, S. Singhala, Appl. Surf. Sci. **324**, 877 (2015)
13. M.A. Nazarkovsky, V.M. Bogatyrov, B. Czech, I.V. Urubkov, E.V. Polshin, G. Wójcik, V.M. Gunko, M.V. Galaburda, J. Skubiszewska-Zięba, J. Photochem. Photobiol. A Chem. **319**, 40 (2016)
14. M. Sajjia, M. Oubaha, M. Hasanuzzaman, A.G. Olabic, Ceram. Int. **40**, 1147 (2014)
15. S. Rasheed, H. Aziz, R. AliKhan, A.M. Khan, A. Rahim, J. Nisar, S. Shah, F. Iqbal, A. Khan, Ceram. Int. **42**, 3666 (2016)
16. R. Safi, A. Ghasemi, R. Shoja-Razavi, M. Tavousi, J. Magn. Magn. Mater. **396**, 288 (2015)
17. J. Saffari, N. Mir, D. Ghanbari, K. Khandan-Barani, A. Hassanabadi, M.R. Hosseini-Tabatabaei, J. Mater. Sci.: Mater. Electron. **26**, 9591 (2015)
18. A. Esmaeili-Bafghi-Karimabad, D. Ghanbari, M. Salavati-Niasari, L. Nejati-Moghadam, S. Gholamrezaei, J. Mater. Sci.: Mater. Electron. **26**, 6970 (2015)
19. D. Ghanbari, S. Sharifi, A. Naraghi, G. Nabiyouni, J. Mater. Sci.: Mater. Electron. **27**, 5315 (2016)
20. A. Shabani, G. Nabiyouni, J. Saffari, D. Ghanbari, J. Mater. Sci. Mater. Electron. **27**, 8661 (2016)
21. M. Masjedi-Arani, M. Salavati-Niasari, Ultrason. Sonochem. **29**, 226 (2016)
22. M. Masjedi-Arani, M. Salavati-Niasari, J. Mater. Sci.: Mater. Electron. **26**, 2316 (2015)
23. M. Masjedi-Arani, M. Salavati-Niasari, Mater. Lett. **174**, 71 (2016)
24. S. Masoumi, G. Nabiyouni, D. Ghanbari, J. Mater. Sci.: Mater. Electron. (2016). doi:10.1007/s10854-016-5067-3
25. S. Masoumi, G. Nabiyouni, D. Ghanbari, J. Mater. Sci.: Mater. Electron. (2016). doi:10.1007/s10854-016-5218-6
26. A. Rezaei, G. Nabiyouni, D. Ghanbari, J. Mater. Sci.: Mater. Electron. (2016). doi:10.1007/s10854-016-5258-y